Counting Active Sites for Nanocatalysis Supplementary Information

Forrest H. Kaatz*[1], Adhemar Bultheel[2], and Dmitry Yu. Murzin[3]

[1]*Institutional Research, NMSU-Alamogordo, 2400 N. Scenic Drive, Alamogordo, NM 88310, USA.*
[2]*Department of Computer Science, KU Leuven, Celestijnenlaan 200A, 3001 Heverlee, Belgium.*
[3]*Industrial Chemistry and Reaction Engineering, Abo Akademi University, Biskopsgatan 8, Turku, 20500 Finland.*
*Corresponding author: email: fhkaatz@gmail.com

Matrix Analysis

We have previously described our definition of adjacency and Euclidean matrices [1, 2]. Briefly, for fcc crystals, the cutoff value is $r_c = 1.41 \cdot r_{\min}$, where $r_{\min}$ is the smallest bond length [3]. Thus,

$$\mathbf{A}(i,j) = \begin{cases} 1, \text{ if } 1 < r_{ij} < r_c \text{ and } i \neq j, \\ 0, \quad \text{otherwise,} \end{cases} \tag{1}$$

describes the adjacency matrix, and

$$\mathbf{E}(i,j) = \begin{cases} r_{ij}, \text{ if } r_{ij} < r_c \text{ and } i \neq j, \\ 0, \quad \text{otherwise,} \end{cases} \tag{2}$$

describes the Euclidean matrix. The term r_{ij} is the Euclidean distance between atoms i and j. We use an adjacency matrix and Euclidean matrix to determine the diameter, D, of the nanostructure [2], where the bond length depends on the average coordination [4]:

$$r(cn) = \frac{2\, r_B}{\left(1 + \exp\left(\frac{12 - \langle cn \rangle_c)}{8 \cdot \langle cn \rangle_c}\right)\right)}. \tag{3}$$

Here r_B is the bulk Pt bond length (0.2775 nm) and $\langle cn \rangle_c$ is the average coordination. The diameter is defined as the maximum distance between atoms in the Euclidean matrix,($\mathbf{E}$). We find a linear relationship between the diameter of the nanostructure and n, the number of shells.

Mass Activity

Planar Site Density: Crystallography Open Database
https://www.crystallography.net/cod/search.html
Pt fcc cif file 1011109 [5]
Software VESTA 3 [6]
Lattice constant Pt: $a = 0.39239$ nm $= 0.39239 \times 10^{-7}$ cm
Area of fcc (100) $A_{100} = a^2$
Area of fcc (111) triangle $A_T = 1/2\ (b \cdot h) = 1/2 \cdot (\sqrt{2} \cdot a \cdot \sqrt{3/2} \cdot a) = \sqrt{3}/2 \cdot a^2$
Planar site density $d_{(100)}$ = atoms/area = (4·(1/4)+1)/area = $\frac{2}{a^2} = 1.2989 \times 10^{15}$ atoms/cm^2

Planar site density $d_{(111)} = (3 \cdot (1/2) + 3 \cdot (1/6))/A_T = \frac{4}{\sqrt{3} \cdot a^2} = 1.500 \times 10^{15}$ atoms/cm^2

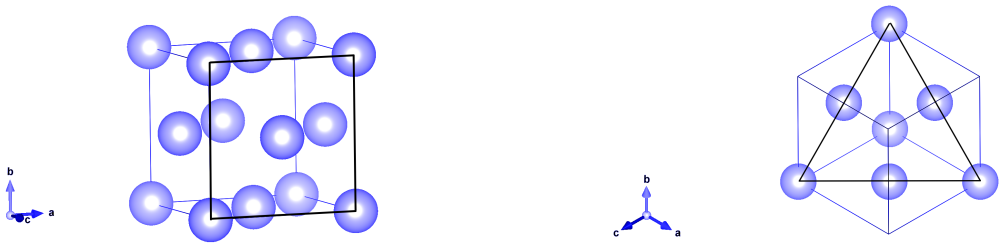

A. B.

Figure 1: A. Pt(100) & B. Pt(111)

We use a model developed by Rück, et al, for the mass activity of platinum nanoparticles [7, 8]. A plot of platinum experimental activity can be described with a volcano plot having a peak in the data. This volcano plot can then be fit to exponential functions of activity versus ($\overline{CN}$). The active sites are those with $7.5 \leq \overline{CN} \leq 8.3$. The exponential fit is described by eq (4) below.

$$A_{volc}(\overline{CN}) = \begin{cases} \exp(3.14\,\overline{CN} - 23.40), & 7.5 \leq \overline{CN} \leq 8.1, \\ \exp(-4.96\,\overline{CN} + 42.18), & 8.1 < \overline{CN} \leq 8.3, \\ 0, & \text{otherwise.} \end{cases} \tag{4}$$

This results in the relative mass activity j_{rel} in (5) (the relative activity from the $\overline{CN}s$ of the structure) below which is the product of the number of atoms $N(\overline{CN}_i)$ and activity A_{volc} for a specified $\overline{CN}_i$

$$j_{rel}(n) = \sum_{i=1}^{N_T(n)} A_{volc}(\overline{CN}_i) = \sum_{7.5 \leq \overline{CN}_i \leq 8.3} N(\overline{CN}_i, n) \cdot A_{volc}(\overline{CN}_i). \tag{5}$$

The mass activity $j_m(n)$ (m is mass, s is specific) is then:

$$j_m(n) = \frac{j_s^0}{d_{Pt} \cdot m_{Pt} \cdot N_T(n)} \cdot j_{rel}(n). \tag{6}$$

Experimentally the bulk values of specific activity j_s^0 for the low index surfaces of Pt are [9]: Pt(100) = 1 mA/cm^2, Pt(111) = 2 mA/cm^2, Pt(110) = 2.45 mA/cm^2. Here $m_{\mathrm{Pt}} = 195.084\,u$, with $u = 1.66054 \times 10^{-21}$ mg the atomic mass unit, while $N_T(n)$ is the cubic polynomial giving the total number of atoms in the cluster and $d_{\mathrm{Pt}} = d_{(100)}$ or $d_{(111)}$ from above.

$$j_m^{\mathrm{Pt}(111)}(n) = \frac{4.116\ \mathrm{A/mg_{Pt}}}{N_T(n)} \cdot \sum_{7.5 \leq \overline{CN}_i \leq 8.3} N(\overline{CN}_i, n) \cdot A_{volc}(\overline{CN}_i), \tag{7}$$

$$j_m^{\mathrm{Pt}(100)}(n) = \frac{2.377\ \mathrm{A/mg_{Pt}}}{N_T(n)} \cdot N(\tfrac{20}{3}, n) \cdot A_{volc}(\tfrac{20}{3}), \tag{8}$$

where the GCN value $20/3 \approx 6.67$ is the (100) facet site and $N(\frac{20}{3}, n)$ is the quadratic polynomial in n, giving the count of sites whose GCN equals 20/3.

We assume the active sites on Pt(100) are the facet sites. To determine $A_{volc}(\frac{20}{3})$, we fit our equation to experimental data. From [10] we have Pt cubes, size 9 nm edge length or ($D = 16$ nm and $n = 24$), have $j_m^{\mathrm{Pt}(100)} = 0.07$ A/mg$_{\mathrm{Pt}}$, $D = 2.4326 \cdot n_B \cdot n - 0.405$, $n_B = 0.2775$ nm. We also have $\frac{N(\frac{20}{3}, n)}{N_T(n)} = \frac{12n^2 - 36n + 6}{4n^3 + 6n^2 + 3n - 7}$ which gives us $A_{volc}(\frac{20}{3}) = 0.286$.

For experimental guidelines for measuring activity see Ref. [11]

Comments on GCNs and methods

From the binary adjacency matrix we compute the coordination number cn_i of site i by summing the elements of row i in $\mathbf{A}$. Our structure consists of $n + 1$ shells numbered $0, 1, \ldots, n$, which in the case of the cages have t inner layers corresponding to shells $n, n - 1, \ldots, n - t + 1$. Since we consider the on-top sites for an fcc structure, we know that $\overline{CN}_{\max} = 12$. Once the cn_i are known for all the sites, we can compute their $\overline{CN}_i$. There is only a limited set of different $\overline{CN}_i$ in a cluster or cage. For a given cluster with n shells, we can compute $N(c, n)$, the number of $\overline{CN}_i$ equal to c. Since $N(c, n)$ depends quadratically on n, we can compute $N(c, n)$ for 3 consecutive (relatively small) values of n, say $n = n_0 + j$, $j = 0, 1, 2$. By solving a 3×3 linear Vandermonde system we can obtain the polynomial coefficients. It has to be verified that by increasing n_0, which is usually equal to 1, the formulas do not change. If the formulas become stable from n_0 on, then we assume they hold for all $n \geq n_0$. To get the exact rational coefficients, one needs to solve the Vandermonde system for the coefficients in exact arithmetic. For a given cluster or cage with n shells, we can compute a magic polynomial, $N(c, n)$, with c equal to a value of $\overline{CN}$. These polynomials compute the count of sites with identical $\overline{CN}$ for larger n. Some of the $\overline{CN}_i$ correspond to active sites which means that we have counts of active sites which contribute to the overall mass activity of the nanostructure. Clearly for nanocages the magic formulas depend not only on n but also on the number of wall layers t. We consider the cases where $3 \leq t \leq 10$, since for thinner walls, the GCNs become smaller and the concept of GCN analysis is not meant for such sub-nano cases [12].

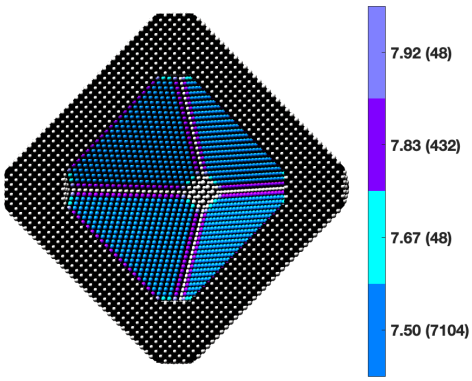

Figure 2: Truncated octahedron (TO) with 7 layers.

The GCNs and counts are given in the colorbar of Fig. 2. Then $j_m^{TO} = (4.116 \cdot 1.1618 \cdot 7104 + 4.116 \cdot 1.961 \cdot 48 + 4.116 \cdot 3.309 \cdot 432 + 4.116 \cdot 4.344 \cdot 48)/31600 = 1.3$ A/mg$_{\mathrm{Pt}}$

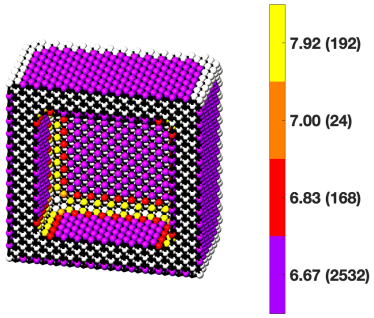

Truncated Cube $t = 5$	
Atoms N_T	$60n^2 - 240n + 358$, $n \geq 8$
$\overline{CN} = \frac{20}{3} = 6.67$	$24n^2 - 192n + 516$, $n \geq 8$
$\overline{CN} = \frac{95}{12} = 7.92$	$24n - 144$, $n \geq 8$

A. Truncated Cube $n = 14, t = 5$ B. Magic formulas for the $\overline{CN}$

Figure 3: Truncated Cube

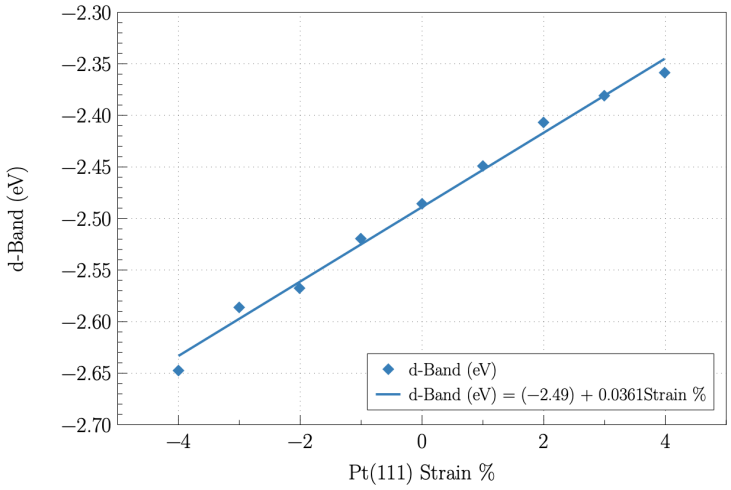

Figure 4: Pt(111) Strain and d-band Center [13]

References

[1] F.H. Kaatz and A. Bultheel. Magic mathematical relationships for nanoclusters. *Nanoscale Res. Letters*, 14(1):150, 2019.

[2] F.H. Kaatz and A. Bultheel. Magical mathematical formulas for nanoboxes. *Nanoscale Res. Letters*, 16:39, 2021.

[3] F.H. Kaatz and A. Bultheel. Magic mathematical relationships for nanoclusters - errata and addendum. *Nanoscale Res. Letters*, 14(1):295, 2019.

[4] C.Q. Sun. Size dependence of nanostructures: Impact of bond order deficiency. *Prog. Solid State Chem.*, 35(1):1–159, 2007.

[5] A.W Hull. X-ray crystal analysis of thirteen common metals. *Physical Review*, 17:571–587, 1921.

[6] K.Momma and F. Izumi. VESTA 3 for three-dimensional visualization of crystal, volumetric and morphology data. *J. Appl. Cryst.*, 44:1272–1276, 2011.

[7] M.Rück, A. Bandarenka, F. Calle-Vallejo, and A. Gagliardi. Oxygen reduction reaction: Rapid prediction of mass activity of nanostructured platinum electrocatalysts. *J. Phys. Chem. Lett.*, 9:4463–4468, 2018.

[8] M.Rück, A. Bandarenka, F. Calle-Vallejo, and A. Gagliardi. Fast identification of optimal pure platinum nanoparticle shapes and sizes for efficient oxygen electroreduction. *Nanoscale Advances*, 1:2901–2909, 2019.

[9] V.R. Stamenkovic, B. Fowler, B.S. Mun, et al. Improved oxygen reduction activity on $Pt_3Ni(111)$ via increased surface site availability. *Science*, 315(5811):493–497, 2007.

[10] S.Xie, S.-I. Choi, N.Lu, et al. Atomic layer-by-layer deposition of Pt on Pd nanocubes for catalysts with enhanced activity and durability toward oxygen reduction. *Nano Lett.*, 14:3570–3576, 2014.

[11] Y. Garsany, O.A. Baturina, K.E. Swider-Lyons, and S.S. Kocha. Experimental methods for quantifying the activity of platinum electrocatalysts for the oxygen reduction reaction. *Anal. Chem*, 82(15):6321–6328, 2010.

[12] F. Calle-Vallejo. The ABC of generalized coordination numbers and their use as a descriptor in electrocatalysis. *Adv. Sci.*, 10(20):2207644, 2023.

[13] H. Wang, S. Hu, C. Tsai, et al. Direct and continuous strain control of catalysts with tunable battery electrode materials. *Science*, 354:1031–1036, 2016.